

FIG. 1. Two different Zeeman slowing schemes for diatomic molecules: (a) laser scheme from Ref.[29] and (b) laser scheme in DSZS. The hyperfine levels of the ground state  $X^2\Sigma_{1/2}$  are separated as two manifolds with  $m_S = \pm 1/2$  respectively. Each manifold has six sublevels. The excited state  $A^2\Pi_{1/2}$  has four sublevels but the  $m_I = \pm 1/2$  states are degenerated since the nuclear spin  $g$ -factor is too small to affect the total Hamiltonian. For SrF molecule in (a), the splitting of the  $m_J = \pm 1/2$  states is negligible while it is not the case for BaF molecule in (b). The wide arrow (red) indicate the frequency-broadened repump laser and the narrow arrows indicate the frequency-modulated slowing laser in (a). In DSZS scheme (b), the wide red arrows are clean-up lasers while the narrow orange arrows are repump laser.

The slowing laser always keeps on- or near-resonance with the main cooling transition to make the particles efficiently slowed during the propagation. Both the type-I and type-II Zeeman slowers share such a basic compensation mechanism. But for type-II ones, the particles may accumulate into the unwanted dark states, making the slowing force vanish. Even if we destabilize the dark states by applying an angled magnetic field [37], the nonlinear energy shifts of the hyperfine sublevels for molecules make the conventional Zeeman slower no longer work well, especially in the weak magnetic field regime. In Ref.[29], a large offset magnetic field  $B_0 \sim 900$  G is introduced to simplify the choice of the cooling and repumping laser components; see Fig.1(a). Under a large magnetic field, the electron spin decouples with the nuclear spin and rotational angular momentum. The sublevels in the ground state now are separated into two manifolds with  $m_S = \pm 1/2$  respectively. The excited state, however, can be regarded as degenerated due to the small  $g$ -factor compared to the ground state [for example, SrF [38] and YO [39] molecules]. This makes the whole system reduce to a simple three-level system. Here, a slowing laser with six frequency sidebands couples the  $m_S = +1/2$  states to the excited states according to the selection rules, while a frequency-broadened laser repumps the molecules that decay to the  $m_S = -1/2$  manifold back to  $m_S = +1/2$  for a wide velocity range. The repump laser must have a rather wide frequency broadening up to about 1 GHz. In order to avoid the influence from the repump laser on the  $m_S = -1/2$  manifold, the

offset magnetic field should be large enough to split the  $m_S = \pm 1/2$  manifolds away from each other. This type-II Zeeman slower has been proved to work as efficiently as the type-I Zeeman slower in a K atom experiment [30].

It is obvious that the scheme only fits for molecules with a small upper  $g$ -factor  $g_\Pi$ , otherwise the simplified three-level model collapses. When  $g_\Pi$  is no longer small enough, the splitting between the upper  $m_{J'} = \pm 1/2$  states is considerably large even under a small magnetic field. Let us revisit the scheme in Fig.1(a), since the energy gap between the two upper  $m_{J'}$  manifolds is large, the resonant frequencies of the six cooling transitions can not change synchronously with the compensations from the magnetic field at the same time, leading to a less efficient slowing. Therefore, we propose the dark state Zeeman slower scheme (DSZS) shown in Fig.1(b), in which the compensation of the Doppler shift is done on the repump laser. Similarly, we still apply an offset magnetic field to let the electron spin decoupled. Instead of applying a slowing laser with six frequencies to couple six hyperfine levels to the excited state, we use a repump laser with two frequencies to couple only two of the levels, which we call the 'selected' states. To ensure the molecules stay in the two 'selected' states, widely broadened clean-up beams are required to couple all the rest ground states at an arbitrary position during the propagation. In this way, it keeps molecules with the "wrong" velocity in the dark states while release them at the "right" velocity to get slowed at a specific position. When molecules with a velocity mismatch the resonant condition, they will be protected in the two 'selected' levels and wait for the Zeeman shift to match again. In the end, the velocity distribution of the molecular beam can be compressed into a sharp and narrow distribution around a tunable final velocity.

To show the advantages of the DSZS scheme in Fig.1(b), we take BaF molecule as an example. We choose the  $|m_S = -1/2, m_N = +1, m_I = \pm 1/2\rangle$  states as the 'selected' states and the laser polarization to be  $\sigma^-$  to make them only coupled to the excited  $|m_{J'} = -1/2, m_{I'} = \pm 1/2\rangle$  states respectively. The polarization of the laser that drives all the other states in the  $m_S = -1/2$  manifold is chosen to be  $\sigma^+$ , such that the selected transitions will not be disturbed by it with a different polarization. Another clean-up laser that drives the ground  $m_S = +1/2$  manifold is also required, and similarly we should apply an offset magnetic field to yield a large energy gap between the two ground manifolds. Because the repump laser and the clean-up lasers interact with the moving molecule independently, there is no need to keep a large energy gap between the  $m_S = \pm 1/2$  manifolds. So the DSZS can effectively work in a relatively smaller magnetic field regime, for example, 300 G  $\sim$  400 G for the BaF molecule. In our scheme, the Landé  $g$ -factor of the excited state is no longer a restriction since the repump laser couples the 'selected' states to the same upper  $m_{J'}$  manifold.

We use the multi-level rate equation approach to calcu-

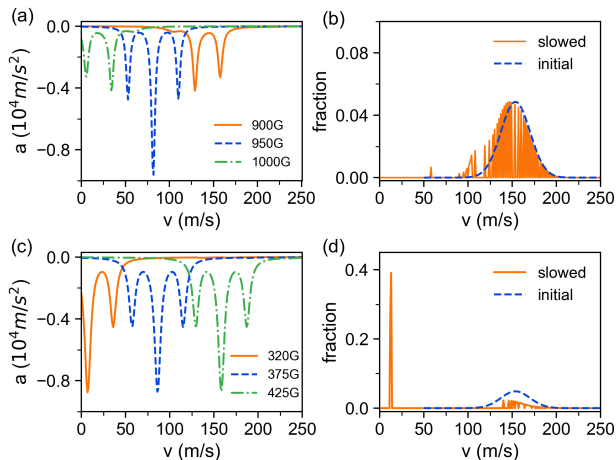


FIG. 2. (a) The velocity-dependent deceleration rate under different magnetic field for the type-II Zeeman slower scheme in Fig.1(a). (b) The initial velocity distribution (blue dotted line) and the final velocity distribution after the deceleration of the type-II Zeeman slower (orange solid line). (c) The velocity dependent deceleration rate under different magnetic field with DSZS scheme shown in Fig.1(b). (d) The initial velocity distribution (blue dotted line) and the final velocity distribution after the deceleration of DSZS (orange solid line).

late the slowing force for different moving velocities, and then simulate the slowing process of a molecular beam with an initial velocity distribution [40]

$$f(v) = Av^2 e^{-\beta(v-v_0)^2} \quad (1)$$

where  $A$  is the normalization parameter,  $\beta$  is related to the temperature and the molecular mass, and  $v_0$  is the center velocity. The multi-level rate equations can be derived from the optical Bloch equation as [41]

$$\begin{aligned} \frac{dN_l}{dt} &= \sum_{u,p} R_{l,u,p}(N_u - N_l) + \Gamma \sum_u r_{l,u} N_u, \\ \frac{dN_u}{dt} &= \sum_{l,p} R_{l,u,p}(N_l - N_u) - \Gamma N_u, \end{aligned} \quad (2)$$

where  $N_u$  and  $N_l$  are the populations of the excited state  $|u\rangle$  and ground state  $|l\rangle$  respectively,  $r_{l,u}$  is the branching ratio of the decay from the upper  $|u\rangle$  state to the ground  $|l\rangle$  state, and  $\Gamma$  is the decay rate of the excited state. The excitation rate from  $|l\rangle$  to  $|u\rangle$  by the  $p$ -th beam is given by

$$R_{l,u,p} = \frac{\Gamma}{2} \frac{s_p}{1 + 4\Delta_{l,u}^2/\Gamma^2} \quad (3)$$

with  $s_p$  is the saturation parameter.  $\Delta_{l,u}$  is the detuning between  $|u\rangle$  and  $|l\rangle$ , including both the Zeeman shift and the Doppler shift. The radiative force can be obtained from the number of the scattered photons, i.e.,

$$F = \sum_{l,u,p} \hbar k_p R_{l,u,p} (N_u - N_l) \quad (4)$$

with  $k_p$  the wavevector of the  $p$ -th beam.

### III. SIMULATION AND COMPARISON

#### A. BaF molecule

The BaF molecule is a candidate for direct laser cooling and the molecular structures and branching ratios have already been investigated in detail [31]. In Fig.2, we show the different slowing results for the BaF molecule with the two schemes mentioned in Fig.1. For the one shown in Fig.1(a), we set the position-dependent magnetic field with the formula [30]

$$B = B_0 + \alpha L(1 - \sqrt{1 - z/L}), \quad (5)$$

in which  $B_0$  is the offset magnetic field,  $\alpha$  is the magnetic field gradient,  $z$  is the position of the molecule and  $L$  is the total length of the slower. Here we set  $L = 1.75$  m,  $B_0 = 900$  G,  $\alpha = 57$  G/m, leading to a maximum magnetic field of  $B_{\max} = 1000$  G. The slowing laser is sideband modulated carefully to be on-resonance with each slowing transition at  $B = 950$  G and the velocity  $v = 80$  m/s. The saturation parameter for each slowing beam is  $s = 8$ , while the repump laser takes  $s = 72$  with a frequency bandwidth of 1.2 GHz.

For DSZS scheme in Fig.1(b), the magnetic field has a monotonically decreasing form

$$B = B_0 + \alpha L \sqrt{1 - z/L}. \quad (6)$$

The difference between the two magnetic field, i.e., Eq.(5) and Eq.(6), comes from the choices of different  $m_S$  quantum numbers of the ground states that do the compensation. The parameters we use here are  $B_0 = 320$  G,  $\alpha = 60$  G/m, and  $L = 1.75$  m. The saturation parameters of two frequency components in the repump laser are  $s = 2$ , and they are set to be on-resonance respectively with the transitions of  $|m_S = -1/2, m_N = +1, m_I = \pm 1/2\rangle \rightarrow |m_{J'} = -1/2, m_{I'} = \pm 1/2\rangle$  at specific position and velocity. The bandwidth of the clean-up laser that pumps the rest states in  $m_S = -1/2$  manifold is broadened to be 400 MHz, and its saturation parameter  $s = 8$ . For the laser that pumps the  $m_S = +1/2$  manifold, the bandwidth is 750 MHz and the saturation parameter  $s = 72$ . The initial velocity distribution centering at 150 m/s (from 50 m/s to 250 m/s) is estimated by Eq.(1) to be a good approximation to the experimental measurement.

As shown in Fig.2(a), when the magnetic field changes, the type-II Zeeman slower scheme in Ref.[29] can not provide a large and stable slowing force for the BaF molecule. As the magnetic field goes away from the center point  $B = 950$  G, the absolute value of the deceleration rate rapidly decreases. The reason lies in that the states in  $m_S = +1/2$  manifold are coupled to different excited states, i.e.,  $|m_S = +1/2, m_N = 0, m_I = \pm 1/2\rangle \rightarrow |m_{J'} = -1/2, m_{I'} = \pm 1/2\rangle$  and  $|m_S = +1/2, m_N = \pm 1, m_I = \pm 1/2\rangle \rightarrow |m_{J'} = +1/2, m_{I'} = \pm 1/2\rangle$ . The energy splittings of the  $m_{J'} = \pm 1/2$  states show different behaviours when the magnetic field increases, resulting in that the

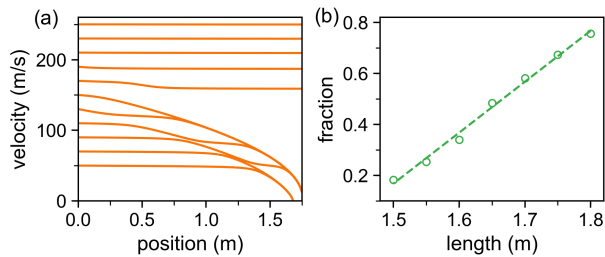


FIG. 3. (a) The position-dependent evolutions of molecules with different initial velocities from 50 m/s to 250 m/s. (b) The dependence of the final compressed molecular fraction below 15 m/s on the length of the Zeeman slower.

slowing laser can not be resonant with the molecules all the time.

The slowing force of our dark state Zeeman slower shows its robustness to the change of the magnetic field; see Fig.2(c). By adjusting the magnetic field, a maximum deceleration rate of  $-8000$  m/s<sup>2</sup> can be achieved. When all the frequency components of the repump beam are on-resonance respectively, no dark state exists and the deceleration rate reaches the maximum value, i.e., the center dip in Fig.2(c). As the velocity changes, the repump beam becomes off resonance. The two *selected* states become dark and the deceleration effect rapidly disappears. However, there is a special case that the Doppler shift only compensates for one frequency component to be resonant while makes the other far detuned. Then, one of the *selected* states becomes dark and only the other one contributes to the photon scattering, resulting in the two weak dips besides the main center dip in Fig.2(c).

A comparison of the slowing effect from the two different schemes is shown in Fig.2. For the old one, with the parameters described above, the final velocity distribution slightly changes, and only a small fraction of BaF molecules are decelerated; see Fig.2(b). However, with our DSZS scheme, the slowing effect gets enhanced. As shown in Fig.2(d), about 66% of the BaF molecules are slowed to a velocity below 15 m/s. Note that here we only consider one-dimensional slowing. In a real slowing experiment, the transverse divergence of the molecular beam should be taken into consideration [42], which will weaken the low-velocity fraction of the molecules. Nevertheless, our simulations here show an effective slowing to make the beam converge to a narrow distribution around a low velocity. Such an enhancement makes it possible to load a MOT with a considerable molecular number.

Figure.3(a) shows the trajectory of the moving molecules with different initial velocities when they pass through the dark state Zeeman slower. Molecules with a velocity larger than  $\sim 170$  m/s always stay in far-off detuning condition and no deceleration happens at all even as the magnetic field changes. For low-velocity molecules, for example, less than 100 m/s, they are protected in the two *selected* states at the early stage of the slowing, and

then get slowed at a specific position where the Doppler shift and the Zeeman shift match with each other. The velocity range in which the molecules can be effectively slowed is determined by both the detuning of the repump laser and the distribution of the magnetic field (i.e., the gradient). The slowing efficiency also depends on the length of the slower. As shown in Fig.3(b), the slowed fraction below 15 m/s increases as the length  $L$  increases. Here the offset magnetic field  $B_0 = 320$  G and the gradient  $\alpha = 60$  G/m are fixed for various length in our simulation. Apparently, longer length leads to that molecules with higher velocity can be slowed down. Another issue is that the Zeeman slower for the BaF molecule should be long enough to get a better efficiency as the radiative force is small compared to some other laser-coolable molecules. In an actual experiment, a suitable compromise of the slower length and the transverse divergence should be taken into account.

## B. SrOH molecule

To demonstrate the universality of our dark state Zeeman slower scheme, we check its applicability on a polyatomic molecule SrOH. The structure of the SrOH is much more complicated than the diatomic molecule for it contains three vibrational modes, including degenerated bending vibrations [44]. Optical cycling on a quasi-closed transition and further sub-Doppler cooling have been realized [35, 45]. Here we work on the main cooling transition, i.e.,  $\tilde{X}^2\Sigma_{1/2} \rightarrow \tilde{A}^2\Pi_{1/2}$  transition. The

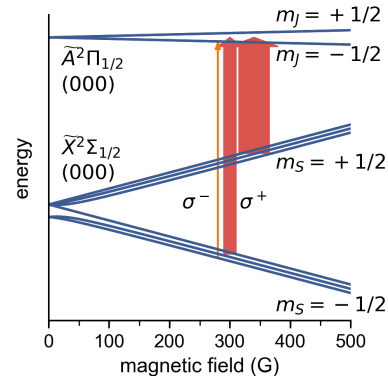


FIG. 4. The structure of the  $\tilde{X}^2\Sigma_{1/2}(000)$  and  $\tilde{A}^2\Pi_{1/2}(000)$  of SrOH molecule (necessary data from Ref.[43]) and the laser scheme applied. The vibrational quantum numbers  $(v_1v_2v_3)$  correspond to the Sr $\leftrightarrow$ OH stretching( $v_1$ ), Sr-O-H bending( $v_2$ ) and SrO $\leftrightarrow$ H stretching( $v_3$ ) vibrational modes. There are 12 sublevels in  $\tilde{X}^2\Sigma_{1/2}(000)$  state but the  $m_I = \pm 1/2$  states are degenerated. A repump laser (the narrow orange arrow) is applied to couple the  $|m_s = -1/2, m_N = 1, m_I = \pm 1/2\rangle$  states with the corresponding excited states. Two clean-up lasers pumps the rest states (the wide red arrows)

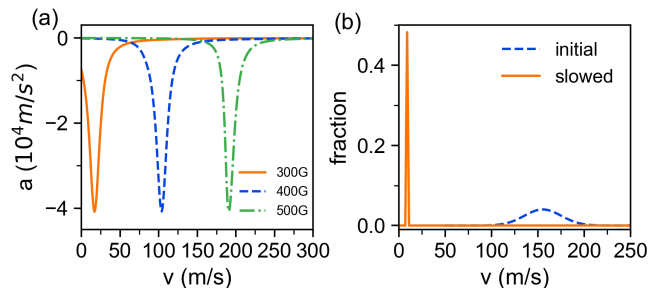


FIG. 5. (a) The deceleration rate versus the velocity under different magnetic field. (b) The initial velocity distribution (blue dotted line) and the final slowed velocity distribution (orange solid line).

splitting between the two  $|m_S, m_N, m_I = \pm 1/2\rangle$  states is about  $\sim 1$  MHz, and they are nearly degenerated, as shown in Fig.4. Here only a single-frequency repump laser is enough, and no sideband modulations are in demand. In our simulation, the repump laser has a saturation parameter of  $s = 2$ , coupling the ground states  $|m_S = -1/2, m_N = 1, m_I = \pm 1/2\rangle$  to  $|m_{J'} = -1/2, m_{I'} = \pm 1/2\rangle$ . The clean-up laser coupling the rest states in the  $m_S = -1/2$  manifold has a saturation parameter of  $s = 8$  and a broadened frequency width of 180 MHz, while another clean-up laser with  $s = 72$  and a broadened bandwidth of 700 MHz.

Figure.5(a) shows the velocity-dependent deceleration rate for the SrOH molecule. The absolute value of deceleration rate can be up to  $-4 \times 10^4$  m/s<sup>2</sup>, which is considerable large enough to slow the molecules. The slowing forces are stable and share a similar shape under different magnetic field strength. This indicates that our scheme can be directly extended to the SrOH molecule. Note that because the repump laser has only one frequency, the deceleration profile under a specific magnetic field only has one dip in Fig.5(a), different from that for the BaF molecule in Fig.2(c).

The distribution of the magnetic field of the slower still follows the formula of Eq.(6), ranging from 540 G to

292 G. The length of the slower is  $L = 1$  m. Figure.5(b) shows the slowing effect. About 99% of the molecules get slowed below 11 m/s without consideration on the transverse divergence. The results discussed above show that the DSZS scheme is capable of slowing polyatomic molecules that has a quasi-closed cycling transition.

#### IV. CONCLUSION

In summary, we propose a general dark state Zeeman slower that can decelerate most species of molecules that can be laser cooled. Compared with the scheme in Ref.[29], such a scheme make it possible to slow molecules that have a relatively large  $g$ -factor of the excited state. Different from the traditional Zeeman slower used in atoms, an offset magnetic field is indispensable, and some clean-up lasers are required to avoid molecules accumulating in dark states. In our scheme, the requirements on the magnetic field and the frequency-broadened clean-up laser are accessible in the current experiments. We extend this scheme to the polyatomic molecule and obtain a good slowing effect with appropriate parameters. Our simulations show that our scheme can efficiently slow molecules to a small velocity under 15 m/s and significantly compress the distribution of the velocity. We expect this dark state Zeeman slower serving as a molecular source to increase the MOT loading rate and molecular number in the future laser-cooling experiments.

#### ACKNOWLEDGMENTS

We acknowledge the support from Nation Natural Science Foundation of China under Grand No.91636104, the National Key Research and Development Program of China under Grand No.2018YFA0307200. Natural Science Foundation of Zhejiang province under Grant No. LZ18A040001, and the Fundamental Research Funds for the Central Universities.

- 
- [1] C. Chin, V. V. Flambaum, and M. G. Kozlov, *New J. Phys* **11**, 055048 (2009).
  - [2] D. DeMille, S. B. Cahn, D. Murphree, D. A. Rahmlow, and M. G. Kozlov, *Phys. Rev. Lett.* **100**, 023003 (2008).
  - [3] M. S. Safronova, D. Budker, D. DeMille, D. F. J. Kimball, A. Derevianko, and C. W. Clark, *Rev. Mod. Phys.* **90**, 025008 (2018).
  - [4] S. Ospelkaus, K.-K. Ni, D. Wang, M. H. G. de Miranda, B. Neyenhuis, G. Quémener, P. S. Julienne, J. L. Bohn, D. S. Jin, and J. Ye, *Science* **327**, 853 (2010).
  - [5] D.-W. Wang, M. D. Lukin, and E. Demler, *Phys. Rev. Lett.* **97**, 180413 (2006).
  - [6] I. Bloch, J. Dalibard, and W. Zwerger, *Rev. Mod. Phys.* **80**, 885 (2008).
  - [7] B. Yan, S. A. Moses, B. Gadway, J. P. Covey, K. R. A. Hazzard, A. M. Rey, D. S. Jin, and J. Ye, *Nature* **501**, 521 (2013).
  - [8] D. DeMille, *Phys. Rev. Lett.* **88**, 067901 (2002).
  - [9] A. André, D. DeMille, J. M. Doyle, M. D. Lukin, S. E. Maxwell, P. Rabl, R. J. Schoelkopf, and P. Zoller, *Nat. Phys* **2**, 636 (2006).
  - [10] A. Micheli, G. K. Brennen, and P. Zoller, *Nat. Phys* **2**, 341 (2006).
  - [11] P. Rabl, D. DeMille, J. M. Doyle, M. D. Lukin, R. J. Schoelkopf, and P. Zoller, *Phys. Rev. Lett.* **97**, 033003 (2006).
  - [12] K.-K. Ni, S. Ospelkaus, M. H. G. de Miranda, A. Pe'er, B. Neyenhuis, J. J. Zirbel, S. Kotochigova, P. S. Julienne, D. S. Jin, and J. Ye, *Science* **322**, 231 (2008).

- [13] J. L. Bohn, A. M. Rey, and J. Ye, *Science* **357**, 1002 (2017).
- [14] J. F. Barry, D. J. McCarron, E. B. Norrgard, M. H. Steinecker, and D. DeMille, *Nature* **512**, 286 (2014).
- [15] A. L. Collopy, S. Ding, Y. Wu, I. A. Finneran, L. Anderegg, B. L. Augenbraun, J. M. Doyle, and J. Ye, *Phys. Rev. Lett.* **121**, 213201 (2018).
- [16] L. Anderegg, B. L. Augenbraun, Y. Bao, S. Burchesky, L. W. Cheuk, W. Ketterle, and J. M. Doyle, *Nat. Phys* **14**, 890 (2018).
- [17] S. Truppe, H. J. Williams, M. Hambach, L. Caldwell, N. J. Fitch, E. A. Hinds, B. E. Sauer, and M. R. Tarbutt, *Nat. Phys* **13**, 1173 (2017).
- [18] S. E. Maxwell, N. Brahms, R. deCarvalho, D. R. Glenn, J. S. Helton, S. V. Nguyen, D. Patterson, J. Petricka, D. DeMille, and J. M. Doyle, *Phys. Rev. Lett.* **95**, 173201 (2005).
- [19] J. F. Barry, E. S. Shuman, E. B. Norrgard, and D. DeMille, *Phys. Rev. Lett.* **108**, 103002 (2012).
- [20] B. Hemmerling, E. Chae, A. Ravi, L. Anderegg, G. K. Drayna, N. R. Hutzler, A. L. Collopy, J. Ye, W. Ketterle, and J. M. Doyle, *J. Phys. B* **49**, 174001 (2016).
- [21] S. Truppe, H. J. Williams, N. J. Fitch, M. Hambach, T. E. Wall, E. A. Hinds, B. E. Sauer, and M. R. Tarbutt, *New J. Phys* **19**, 022001 (2017).
- [22] M. Yeo, M. T. Hummon, A. L. Collopy, B. Yan, B. Hemmerling, E. Chae, J. M. Doyle, and J. Ye, *Phys. Rev. Lett.* **114**, 223003 (2015).
- [23] V. Zhelyazkova, A. Cournol, T. E. Wall, A. Matsushima, J. J. Hudson, E. A. Hinds, M. R. Tarbutt, and B. E. Sauer, *Phys. Rev. A* **89**, 053416 (2014).
- [24] A. Prehn, M. Ibrügger, R. Glöckner, G. Rempe, and M. Zeppenfeld, *Phys. Rev. Lett.* **116**, 063005 (2016).
- [25] E. Narevicius, A. Libson, C. G. Parthey, I. Chavez, J. Narevicius, U. Even, and M. G. Raizen, *Phys. Rev. Lett.* **100**, 093003 (2008).
- [26] S. Y. van de Meerakker, N. Vanhaecke, and G. Meijer, *Ann. Rev. Phys. Chem.* **57**, 159 (2006).
- [27] M. Zhu, C. W. Oates, and J. L. Hall, *Phys. Rev. Lett.* **67**, 46 (1991).
- [28] W. Ertmer, R. Blatt, J. L. Hall, and M. Zhu, *Phys. Rev. Lett.* **54**, 996 (1985).
- [29] M. Petzold, P. Kaebert, P. Gersema, M. Siercke, and S. Ospelkaus, *New J. Phys* **20**, 042001 (2018).
- [30] M. Petzold, P. Kaebert, P. Gersema, T. Poll, N. Reinhardt, M. Siercke, and S. Ospelkaus, *Phys. Rev. A* **98**, 063408 (2018).
- [31] T. Chen, W. Bu, and B. Yan, *Phys. Rev. A* **94**, 063415 (2016).
- [32] W. Bu, T. Chen, G. Lv, and B. Yan, *Phys. Rev. A* **95**, 032701 (2017).
- [33] T. Chen, W. Bu, and B. Yan, *Phys. Rev. A* **96**, 053401 (2017).
- [34] I. Kozyryev, L. Baum, K. Matsuda, P. Olson, B. Hemmerling, and J. M. Doyle, *New J. Phys* **17**, 045003 (2015).
- [35] I. Kozyryev, L. Baum, K. Matsuda, B. Hemmerling, and J. M. Doyle, *J. Phys. B* **49**, 134002 (2016).
- [36] W. D. Phillips and H. Metcalf, *Phys. Rev. Lett.* **48**, 596 (1982).
- [37] D. J. Berkeland and M. G. Boshier, *Phys. Rev. A* **65**, 033413 (2002).
- [38] E. S. Shuman, J. F. Barry, and D. DeMille, *Nature* **467**, 820 (2010).
- [39] M. T. Hummon, M. Yeo, B. K. Stuhl, A. L. Collopy, Y. Xia, and J. Ye, *Phys. Rev. Lett.* **110**, 143001 (2013).
- [40] S. Truppe, M. Hambach, S. M. Skoff, N. E. Bulleid, J. S. Bumby, R. J. Hendricks, E. A. Hinds, B. E. Sauer, and M. R. Tarbutt, *J. Mod. Opt.* **65**, 648 (2018).
- [41] M. O. Scully and M. S. Zubairy, *Quantum Optics* (Cambridge University Press, 1997).
- [42] J. F. Barry, E. S. Shuman, and D. DeMille, *Phys. Chem. Chem. Phys.* **13**, 18936 (2011).
- [43] D. A. Fletcher, K. Y. Jung, C. T. Scurlock, and T. C. Steimle, *J. Chem. Phys.* **98**, 1837 (1993).
- [44] P. I. Presunka and J. A. Coxon, *Chem. Phys* **190**, 97 (1995).
- [45] I. Kozyryev, L. Baum, K. Matsuda, B. L. Augenbraun, L. Anderegg, A. P. Sedlack, and J. M. Doyle, *Phys. Rev. Lett.* **118**, 173201 (2017).